

Heavy-Higgs Lifetime at Two Loops

A. FRINK¹, B.A. KNIEHL^{2,*}, D. KREIMER¹, AND K. RIESELMANN³

¹ Institut für Physik, Johannes-Gutenberg-Universität,
Staudinger Weg 7, 55099 Mainz, Germany

² Institut für Theoretische Physik, Ludwig-Maximilians-Universität,
Theresienstraße 37, 80333 München, Germany

³ Institut für Theoretische Physik, Technische Universität München,
James-Frank-Straße, 85747 Garching, Germany

Abstract

The Standard-Model Higgs boson with mass $M_H \gg 2M_Z$ decays almost exclusively to pairs of W and Z bosons. We calculate the dominant two-loop corrections, of $O(G_F^2 M_H^4)$, to the partial widths of these decays. In the on-mass-shell renormalization scheme, the correction factor is found to be $1 + 14.6\%(M_H/\text{TeV})^2 + 16.9\%(M_H/\text{TeV})^4$, where the second term is the one-loop correction. We give full analytic results for all divergent two-loop Feynman diagrams. A subset of finite two-loop vertex diagrams is computed to high precision using numerical techniques. We find agreement with a previous numerical analysis. The above correction factor is also in line with a recent lattice calculation.

PACS numbers: 12.15.Lk, 14.70.Fm, 14.70.Hp, 14.80.Bn

*Permanent address: Max-Planck-Institut für Physik (Werner-Heisenberg-Institut), Föhringer Ring 6, 80805 Munich, Germany.

1 Introduction

One of the longstanding questions of elementary particle physics is whether nature makes use of the Higgs mechanism of spontaneous symmetry breaking to endow the particles with their masses. The Higgs boson, H , is the missing link sought to verify this theoretical concept in the Standard Model (SM). Its mass, M_H , is essentially a free parameter of the SM. The failure of experiments at the CERN Large Electron-Positron Collider (LEP 1) and the SLAC Linear Collider (SLC) to observe the decay $Z \rightarrow f\bar{f}H$ has ruled out the mass range $M_H \leq 65.2$ GeV at the 95% confidence level [1]. The discovery potential of LEP 2, with centre-of-mass (c.m.) energy $\sqrt{s} = 192$ GeV and luminosity $L = 150$ pb $^{-1}$ per experiment, will reach up to $M_H \approx 95$ GeV [2]. We note in passing that M_H lower bounds may also be derived theoretically by demanding that the Higgs vacuum be (meta)stable [3].

Several theoretical arguments bound M_H from above. The requirement that partial-wave unitarity in intermediate-boson scattering at high energies be satisfied at tree level establishes an upper bound on M_H at about $(8\pi\sqrt{2}/3G_F)^{1/2} \approx 1$ TeV [4]. This unitarity bound is significantly lowered by including one- [5] and two-loop [6] corrections. However, the improved bound depends on the energy scale, Λ , up to which the SM is assumed to remain valid. The same is true for the triviality bound, which is derived perturbatively [7] by requiring that the running Higgs self-coupling, $\lambda(\mu)$, stays finite for renormalization scales $\mu < \Lambda$. Lattice computations, which take all orders of the perturbative expansion into account, yield a triviality bound of $M_H \approx 700$ GeV [8]. The precise value of this bound depends on the specific form of the lattice action and the regularization method used.

An alternative way of constraining M_H from above is to require that the Higgs sector be weakly interacting, so that perturbation theory is meaningful [9]. The resulting bounds depend somewhat on the considered process and the precise definition of perturbation-theory breakdown, but they are independent of assumptions concerning the scale Λ beyond which new physics operates. At one and two loops, the leading high- M_H corrections to physical observables related to Higgs-boson production or decay are of $O(G_F M_H^2)$ and $O(G_F^2 M_H^4)$, respectively. The one-loop corrections to the partial widths of the Higgs-boson decays to pairs of fermions [10] and intermediate bosons [11] are relatively modest, below 15% at $M_H = 1$ TeV if the on-mass-shell renormalization scheme is employed. The situation is similar for Higgs-boson production [12]. For M_H increasing, the $O(G_F^2 M_H^4)$ corrections will eventually exceed the $O(G_F M_H^2)$ ones in size. In the case of the fermionic Higgs-boson decays, this happens at $M_H \approx 1.1$ TeV in the on-shell scheme [13,14]. Obviously, the perturbative expansion in $G_F M_H^2$ ceases to usefully converge for larger values of M_H . The study of high-energy weak-boson scattering at two loops (with neglect of trilinear couplings) leads to a perturbative upper bound on M_H which depends on the considered c.m. energy. For \sqrt{s} in the 1-TeV range, the M_H upper bound comes out as low as 450 GeV [15]. However, this result may be relaxed using resummation techniques [16].

Since a Higgs boson with $M_H \gg 2M_Z$ decays almost exclusively to W^+W^- and ZZ

pairs, it is desirable, both from the theoretical and phenomenological points of view, to find the two-loop $O(G_F^2 M_H^4)$ corrections to the partial widths of these decays as well. This is the purpose of the present paper. In contrast to the fermionic case [13,14], this involves the calculation of massive three-point functions at two loops. Due to the presence of a large external momentum, heavy-mass expansion techniques are not applicable here. As in a previous analysis [13], we take advantage of the Goldstone-boson equivalence theorem [17] and neglect the gauge and Yukawa couplings as well as the intermediate-boson masses. In this approximation, the radiative corrections to the $H \rightarrow W^+W^-$ and $H \rightarrow ZZ$ decay widths coincide.

In the evaluation of the relevant two-loop Feynman diagrams, both infrared (IR) and ultraviolet (UV) divergences occur. We calculate all divergent diagrams analytically, using dimensional regularization. This guarantees that the cancellation of the IR and UV divergences is manifest. The remaining diagrams are individually devoid of singularities. They are computed numerically in four space-time dimensions after formulating the integrals in parallel and orthogonal space. This has the advantage that potential numerical instabilities in connection with the conventional Feynman parameterizations are avoided. We list our results for the individual diagrams, so that they are available to other authors for comparisons and further calculations.

We anticipate that we find good agreement with a recent, pioneering work by Ghinculov [18], which fully resorts to numerical methods. In Ref. [18], the IR divergences are regularized by introducing a small Goldstone-boson mass. The final result is obtained by numerically taking the massless limit. Another conceptual difficulty in Ref. [18] is related to the treatment of (endpoint) singularities in the Feynman-parameter integrals. These are controlled by choosing suitable integration paths in the complex plane with the aid of spline functions. The values of the individual diagrams are not specified in Ref. [18]. We believe that, in view of the enormous complexity of the problem at hand, it is indispensable to have at least two independent analyses that agree with each other.

This paper is organized as follows. In Sec. 2, we catalogue the contributing Feynman-graph topologies and explain our renormalization framework. In Sec. 3, we describe our analytical and numerical techniques. In Sec. 4, we present our results for the individual two-loop vertex diagrams and assemble the renormalized $H \rightarrow VV$ ($V = W, Z$) transition amplitude. In Sec. 5, we explore the phenomenological implications of our result and draw the conclusions. The relevant one-loop three-point amplitudes to $O(\epsilon)$, where $D = 4 - 2\epsilon$ is the dimensionality of space time, are listed in the Appendix.

2 Framework

In this section, we set the stage for our calculation of the $H \rightarrow VV$ ($V = W, Z$) decay widths to $O(G_F^2 M_H^4)$. As mentioned in the Introduction, this task may be greatly simplified in the limit of interest, $M_H \gg 2M_Z$, through the use of the Goldstone-boson equivalence theorem [17]. This theorem states that the leading high- M_H electroweak contribution to a Feynman diagram may be calculated by replacing the intermediate bosons

W^\pm , Z with the would-be Goldstone bosons w^\pm , z of the symmetry-breaking sector of the theory. In this limit, the gauge and Yukawa couplings may be neglected against the Higgs self-coupling. By the same token, the Goldstone bosons may be taken to be massless, and the fermion loops may be omitted.

Adopting the conventions of Ref. [19], we may write the relevant Lagrangian for the symmetry-breaking sector of the SM in terms of bare quantities, marked by the subscript 0, as

$$\begin{aligned} \mathcal{L}_0^{\text{SBS}} = & \frac{1}{2} \partial_\mu \mathbf{w}_0 \cdot \partial^\mu \mathbf{w}_0 + \frac{1}{2} \partial_\mu H_0 \partial^\mu H_0 - \frac{1}{2} M_{w,0}^2 \mathbf{w}_0^2 - \frac{1}{2} M_{H,0}^2 H_0^2 \\ & - \frac{\lambda_0}{4} (\mathbf{w}_0^2 + H_0^2)^2 - \lambda_0 v_0 (\mathbf{w}_0^2 + H_0^2) H_0, \end{aligned} \quad (1)$$

where λ is the Higgs quartic coupling, v is the Higgs vacuum expectation value, H is the real scalar Higgs field, and the real scalar SO(3) triplet, $\mathbf{w} = (w_1, w_2, w_3)$, is related to the Goldstone bosons, w^\pm and z , by $w^\pm = (w_1 \mp i w_2)/\sqrt{2}$ and $z = w_3$, respectively. The tadpole counterterm, which cancels all tadpole contributions of $\mathcal{L}_0^{\text{SBS}}$ order by order, has been omitted in writing Eq. (1). Consequently, all diagrams which include tadpole contributions need to be dropped in calculations [19].

We work in the on-mass-shell renormalization scheme as formulated in Refs. [13,19]. The residual SO(3) symmetry present in Eq. (1) is preserved in the renormalization procedure, so that the w^\pm and z bosons share one mass counterterm and one wave-function renormalization constant. Specifically, the renormalization conditions are as follows: (i) The mass counterterms, δM_w^2 and δM_H^2 , are determined so that the renormalized masses, $M_w^2 = M_{w,0}^2 - \delta M_w^2$ and $M_H^2 = M_{H,0}^2 - \delta M_H^2$, coincide with the physical (pole) masses, *i.e.*, the pole positions of the radiatively corrected propagators. In the case of the Goldstone bosons, one has $M_w^2 = 0$. (ii) The wave-function renormalization constants, Z_w and Z_H , which enter the relations $w_0^\pm = Z_w^{1/2} w^\pm$ and $H_0 = Z_H^{1/2} H$ between the bare and renormalized fields are adjusted so that the on-shell propagators have unit residues. (iii) The physical Higgs quartic coupling and vacuum expectation value are fixed by requiring that $\lambda = G_F M_H^2/\sqrt{2}$ and $v = 2^{-1/4} G_F^{-1/2}$, respectively, where G_F is Fermi's constant. This leads to the following relations [13,19]:

$$\begin{aligned} \delta M_w^2 &= -\Pi_w^0(0), \\ \delta M_H^2 &= -\text{Re}\Pi_H^0(M_H^2), \\ \frac{1}{Z_w} &= 1 - \left. \frac{d}{dp^2} \Pi_w^0(p^2) \right|_{p^2=0}, \\ \frac{1}{Z_H} &= 1 - \left. \frac{d}{dp^2} \text{Re}\Pi_H^0(p^2) \right|_{p^2=M_H^2}, \\ \lambda_0 &= \frac{\lambda}{Z_w} \left(1 + \frac{\delta M_H^2 - \delta M_w^2}{M_H^2} \right), \\ v_0 &= Z_w^{1/2} v, \end{aligned} \quad (2)$$

where $\Pi_w^0(p^2)$ and $\Pi_H^0(p^2)$ are the self-energy functions of the bare Goldstone and Higgs

fields, respectively, calculated from Lagrangian (1). Two-loop expressions for δM_w^2 , δM_H^2 , Z_w , Z_H , and λ_0 in terms of M_H and λ may be found in Refs. [19,20].

The Feynman diagrams that contribute to the $H \rightarrow VV$ transition amplitude through $O(G_F^2 M_H^4)$ are depicted in Fig. 1. Dashed and solid lines represent Goldstone and Higgs bosons, respectively. Adjacent propagators with identical four-momenta, which occur in connection with mass-counterterm insertions, are separated by solid circles. The calligraphic labels stand for the values of the diagrams and are used in our formulas; the nomenclature extends the one introduced in Ref. [19]. The underlying conventions are explained in Sec. 3 and the Appendix.

There are 6 one-loop diagrams (\mathcal{Q} , \mathcal{B}_i , and \mathcal{C}_i), 18 reducible two-loop diagrams ($\mathcal{B}_i\mathcal{B}_j$, $\mathcal{B}_i\mathcal{C}_j$, $\mathcal{Q}\mathcal{T}_i$, and $\mathcal{Q}\mathcal{D}_i$), and 52 irreducible two-loop diagrams (\mathcal{A}_i , \mathcal{E}_i , \mathcal{L}_i , \mathcal{F}_i , \mathcal{G}_i , \mathcal{H}_i , \mathcal{I}_i , \mathcal{J}_i , and \mathcal{K}_i). In addition, there are 8 one-loop diagrams with one mass-counterterm insertion ($\delta M_a^2\mathcal{T}_i$ and $\delta M_a^2\mathcal{D}_i$, where $a = w, H$). Further reducible two-loop diagrams emerge as products of one-loop vertex and wave-function-renormalization diagrams; these are not counted here. The one-loop diagrams need to be evaluated through $O(\epsilon)$. The corresponding results for the tadpole (\mathcal{Q}) and two-point topologies (\mathcal{B}_i and \mathcal{T}_i) may be found in Ref. [19]; those for the three-point topologies (\mathcal{C}_i and \mathcal{D}_i) are listed in the Appendix. The irreducible two-loop two-point topologies (\mathcal{A}_i , \mathcal{E}_i , and \mathcal{L}_i) may be taken from Ref. [19]. Here, we regard two external legs that merge into the same vertex as one point; solid circles are not counted as points. For example, we view both \mathcal{T}_i and \mathcal{A}_i as two-point topologies.

The main technical difficulty of the present paper is to tackle the irreducible two-loop three-point topologies (\mathcal{F}_i , \mathcal{G}_i , \mathcal{H}_i , \mathcal{I}_i , \mathcal{J}_i , and \mathcal{K}_i). Topologies \mathcal{F}_i , \mathcal{G}_i , and \mathcal{H}_i are ultraviolet divergent. Topologies \mathcal{H}_3 and \mathcal{H}_4 are also plagued by infrared singularities. Topologies \mathcal{I}_i , \mathcal{J}_i , and \mathcal{K}_i are UV and IR finite. After describing our computational techniques in Sec. 3, we itemize the results for topologies \mathcal{F}_1 through \mathcal{K}_2 in Sec. 4.

Calculating the combinatorial factors with the help of the software package DIAGRAMMAR [21], we find the following master formula for the two-loop $H \rightarrow VV$ transition amplitude in terms of λ_0 , v_0 , and M_H :

$$\begin{aligned}
\mathcal{T}(H \rightarrow VV) = & -2\lambda_0 v_0 Z_w Z_H^{1/2} \left\{ 1 + i\lambda_0(10\mathcal{B}_0 + 8\mathcal{B}_1 + 6\mathcal{B}_2) + i(\lambda_0 v_0)^2(8\mathcal{C}_1 + 24\mathcal{C}_2) \right. \\
& - \lambda_0^2(50\mathcal{B}_0\mathcal{B}_0 + 36\mathcal{B}_0\mathcal{B}_2 + 16\mathcal{B}_1\mathcal{B}_1 + 18\mathcal{B}_2\mathcal{B}_2 + 20\mathcal{Q}\mathcal{T}_0 + 8\mathcal{Q}\mathcal{T}_1 + 24\mathcal{Q}\mathcal{T}_2 + 36\mathcal{Q}\mathcal{T}_3 \\
& \quad + 40\mathcal{A}_{10} + 40\mathcal{A}_{1m} + 16\mathcal{A}_{20} + 12\mathcal{A}_{2m} + 24\mathcal{A}_3 + 36\mathcal{A}_4 \\
& \quad \left. + 60\mathcal{F}_1 + 4\mathcal{F}_2 + 24\mathcal{F}_3 + 40\mathcal{F}_4 + 16\mathcal{F}_5 + 24\mathcal{F}_6) \right. \\
& - \lambda_0(\lambda_0 v_0)^2(40\mathcal{B}_0\mathcal{C}_1 + 24\mathcal{B}_0\mathcal{C}_2 + 32\mathcal{B}_1\mathcal{C}_1 + 96\mathcal{B}_1\mathcal{C}_2 + 24\mathcal{B}_2\mathcal{C}_1 + 72\mathcal{B}_2\mathcal{C}_2 \\
& \quad + 16\mathcal{Q}\mathcal{D}_1 + 24\mathcal{Q}\mathcal{D}_{2a} + 24\mathcal{Q}\mathcal{D}_{2b} + 144\mathcal{Q}\mathcal{D}_3 \\
& \quad + 80\mathcal{E}_1 + 32\mathcal{E}_2 + 48\mathcal{E}_2^* + 72\mathcal{E}_3 + 144\mathcal{E}_4 + 216\mathcal{E}_5 \\
& \quad + 40\mathcal{L}_1 + 32\mathcal{L}_{20} + 144\mathcal{L}_{2m} + 96\mathcal{L}_3 + 216\mathcal{L}_5 \\
& \quad + 288\mathcal{G}_1 + 288\mathcal{G}_2 + 64\mathcal{G}_3 + 96\mathcal{G}_4 + 48\mathcal{G}_5 + 80\mathcal{G}_6 \\
& \quad + 48\mathcal{I}_1 + 48\mathcal{I}_2 + 32\mathcal{I}_3 + 288\mathcal{I}_4 + 160\mathcal{I}_5 + 96\mathcal{I}_6 + 32\mathcal{I}_7) \\
& \left. - (\lambda_0 v_0)^4(864\mathcal{H}_1 + 288\mathcal{H}_2 + 64\mathcal{H}_3 + 96\mathcal{H}_4 + 144\mathcal{H}_5 + 48\mathcal{H}_6 + 288\mathcal{K}_1 + 32\mathcal{K}_2) \right\}
\end{aligned}$$

$$\begin{aligned}
& + 864\mathcal{J}_1 + 96\mathcal{J}_2 + 96\mathcal{J}_3 + 32\mathcal{J}_4 + 576\mathcal{J}_5 + 192\mathcal{J}_6 + 192\mathcal{J}_7 + 64\mathcal{J}_8) \\
& + \left[i\lambda_0(20\mathcal{T}_0 + 8\mathcal{T}_1) + i(\lambda_0 v_0)^2(16\mathcal{D}_1 + 24\mathcal{D}_{2b}) \right] \delta M_w^2 \\
& + \left[i\lambda_0(8\mathcal{T}_2 + 12\mathcal{T}_3) + i(\lambda_0 v_0)^2(8\mathcal{D}_{2a} + 48\mathcal{D}_3) \right] \delta M_H^2 \}. \tag{3}
\end{aligned}$$

Here, the tree-level term has been factored out together with the wave-function renormalization constants of the external legs; in our two-loop approximation, these quantities need to be evaluated through $O(\lambda^2)$. The second and third terms within the curly bracket arise at one loop; their prefactors of λ_0 and v_0 need only to be expanded through $O(\lambda)$. The residual terms are of genuine two-loop order; here, λ_0 and v_0 may immediately be replaced with λ and v , and it is sufficient to insert the one-loop expressions for δM_w^2 and δM_H^2 . Notice that we have already performed mass renormalization in Eq. (3), so that M_H , which appears inside the expressions for the various diagrams, is the only mass parameter left.

3 Computational techniques

As usual, we calculate the Feynman diagrams in $D = 4 - 2\epsilon$ space-time dimensions and introduce an unphysical 't Hooft mass scale, μ , to keep the Higgs quartic coupling dimensionless. After coupling renormalization, Eq. (3) will be finite and μ independent in the physical limit $\epsilon \rightarrow 0$. To fix the notation, we write down the generic one-loop two-point integral (with two scalar propagators):

$$\mathcal{B}(p^2, m_1^2, m_2^2) = \mu^{2\epsilon} \int \frac{d^D q}{(2\pi)^D} \frac{1}{(q^2 - m_1^2 + i\epsilon)[(q+p)^2 - m_2^2 + i\epsilon]}. \tag{4}$$

The one-loop two-point diagrams in Fig. 1 are then defined as

$$\begin{aligned}
\mathcal{B}_0 &= \mathcal{B}(M_H^2, 0, 0), \\
\mathcal{B}_1 &= \mathcal{B}(0, 0, M_H^2), \\
\mathcal{B}_2 &= \mathcal{B}(M_H^2, M_H^2, M_H^2), \\
\mathcal{T}_0 &= \frac{\partial}{\partial m_1^2} \mathcal{B}(M_H^2, 0, 0), \\
\mathcal{T}_1 &= \frac{\partial}{\partial m_1^2} \mathcal{B}(0, 0, M_H^2), \\
\mathcal{T}_2 &= \frac{\partial}{\partial m_2^2} \mathcal{B}(0, 0, M_H^2), \\
\mathcal{T}_3 &= \frac{\partial}{\partial m_1^2} \mathcal{B}(M_H^2, M_H^2, M_H^2). \tag{5}
\end{aligned}$$

Analytic results for these diagrams to $O(\epsilon)$ may be found in Ref. [19]. Note that, in contrast to Ref. [19], we exclude the factors of i connected with the scalar propagators in the definitions of the diagrams. For the one-loop tadpole diagram, we have $\mathcal{Q} = M_H^2 \mathcal{B}_1$.

The one-loop three-point diagrams, \mathcal{C}_i and \mathcal{D}_i , are defined and evaluated to $O(\epsilon)$ in the Appendix.

The two-loop diagrams are defined in analogy to Eqs. (4) and (22). We first consider the IR-finite two-loop diagrams in Fig. 1. In the limit $\epsilon \rightarrow 0$, any member, \mathcal{M} , of this class may be cast into the generic form

$$\mathcal{M} = \frac{1}{(4\pi)^4 (M_H^2)^{N-4}} \left(\frac{4\pi\mu^2}{M_H^2 e^\gamma} \right)^{2\epsilon} \left[\frac{A}{\epsilon^2} + \frac{B}{\epsilon} + C + O(\epsilon) \right], \quad (6)$$

where γ is the Euler-Mascheroni constant, N is the number of propagators in \mathcal{M} , and A , B , and C are finite, complex numbers. The special form of the prefactor is to suppress the appearance of the familiar term $\ln(4\pi) - \gamma$ in B and C . (By contrast, the γ piece of the prefactor was expanded in Ref. [19].) Coefficients A , B , and C for diagrams \mathcal{A}_i , \mathcal{E}_i , and \mathcal{L}_i are available in analytic form [19]. Diagrams \mathcal{E}_1 and \mathcal{E}_2 are IR divergent and will be discussed further below.

The irreducible two-loop three-point diagrams with four propagators, \mathcal{F}_i , exhibit UV divergences in the form of quadratic and linear poles in ϵ , but they are IR safe. They may be evaluated analytically from appropriate Feynman-parameter representations, proceeding along the lines of Ref. [19]. In the case of diagram \mathcal{F}_1 , where all internal lines are massless, we find agreement with Ref. [22].

Diagrams \mathcal{G}_i and \mathcal{H}_i are more involved, and it is advantageous to apply dispersion relations in a way similar to Ref. [23]. Let us first concentrate on diagrams \mathcal{G}_i . We observe that they contain a one-loop two-point subdiagram consisting of a bubble and an adjacent propagator. Calling the masses inside this bubble m_1 and m_2 , the mass of the adjacent leg m_3 , and the common four-momentum q , we may rewrite this subdiagram as

$$\frac{\mathcal{B}(q^2, m_1^2, m_2^2)}{q^2 - m_3^2 + i\epsilon} = \frac{\mathcal{B}(m_3^2, m_1^2, m_2^2)}{q^2 - m_3^2 + i\epsilon} - \frac{i}{(4\pi)^2} \int_{(m_1+m_2)^2}^{\infty} \frac{ds}{s} \frac{\sqrt{\lambda(s, m_1^2, m_2^2)}}{s - m_3^2 - i\epsilon} \frac{1}{q^2 - s + i\epsilon} + O(\epsilon), \quad (7)$$

where $\lambda(s, m_1^2, m_2^2) = [s - (m_1 + m_2)^2][s - (m_1 - m_2)^2]$ is the Källén function. If Eq. (7) is inserted in the expression for the one-loop seed diagram, the first term turns into a product of the type $\mathcal{B}_i \mathcal{C}_j$, which contains all divergences. In the second term, we may interchange the dispersion and loop integrations and are left with a finite dispersion integral, which may be solved analytically.

Diagrams \mathcal{H}_i may be treated in a similar fashion. They contain a one-loop two-point subdiagram consisting of a bubble and two identical adjacent propagators. A useful representation of this subdiagram emerges by differentiating Eq. (7) with respect to m_3^2 . The divergences of diagrams \mathcal{H}_i are contained in products of the form $\mathcal{B}_i \mathcal{D}_j$. In particular, this method allows us to separate the IR divergences of diagrams \mathcal{H}_3 and \mathcal{H}_4 . By the way, this method may also be applied to the IR-divergent diagrams \mathcal{E}_1 and \mathcal{E}_2 .

Let us now turn to the cancellation of the IR divergences in Eq. (3). It is possible to extract the IR divergences along with the UV ones as poles in ϵ using dimensional regularization. In fact, this avenue was taken in Ref. [19]. Here, we adopt an alternative strategy. We identify a basic set of IR-divergent one-loop diagrams and show that their

prefactors vanish. In this way, we do not need to solve any IR-divergent loop integral. It is easy to see that the diagrams which emerge by duplicating any of the Goldstone-boson propagators in diagrams \mathcal{B}_0 , \mathcal{B}_1 , \mathcal{C}_1 , and \mathcal{C}_2 are IR divergent. The resulting diagrams are \mathcal{T}_0 , \mathcal{T}_1 , \mathcal{D}_1 , and \mathcal{D}_{2b} , respectively. As for the irreducible two-loop diagrams, \mathcal{E}_1 , \mathcal{E}_2 , \mathcal{H}_3 , and \mathcal{H}_4 are IR divergent. Hence there are twelve IR-divergent terms in Eq. (3). By means of the dispersion-relation method described above, we find that $\mathcal{E}_1 - \mathcal{B}_1\mathcal{T}_0$, $\mathcal{E}_2 - \mathcal{B}_1\mathcal{T}_1$, $\mathcal{H}_3 - \mathcal{B}_1\mathcal{D}_1$, and $\mathcal{H}_4 - \mathcal{B}_1\mathcal{D}_{2b}$ are finite. Exploiting the one-loop identity [19]

$$i\delta M_w^2 = \lambda\mathcal{Q} + 4(\lambda v)^2\mathcal{B}_1, \quad (8)$$

it follows on that the twelve IR-divergent terms in Eq. (3) may be grouped in four finite sets. Specifically, we have

$$\begin{aligned} (\lambda\mathcal{Q} - i\delta M_w^2)\mathcal{T}_0 + 4(\lambda v)^2\mathcal{E}_1 &= \lambda[-2\zeta(2) + 1 - i\pi + O(\epsilon)], \\ (\lambda\mathcal{Q} - i\delta M_w^2)\mathcal{T}_1 + 4(\lambda v)^2\mathcal{E}_2 &= \lambda[-2 + O(\epsilon)], \\ (\lambda\mathcal{Q} - i\delta M_w^2)\mathcal{D}_1 + 4(\lambda v)^2\mathcal{H}_3 &= \frac{1}{v^2} \left[\frac{3}{8}\zeta(2) - \frac{1}{2} + i\frac{\pi}{2} \ln 2 + O(\epsilon) \right], \\ (\lambda\mathcal{Q} - i\delta M_w^2)\mathcal{D}_{2b} + 4(\lambda v)^2\mathcal{H}_4 &= \frac{1}{v^2} \left[-\frac{\zeta(2)}{12} - \frac{\sqrt{3}}{2} \text{Cl}_2\left(\frac{\pi}{3}\right) + \frac{\pi}{2\sqrt{3}} + \frac{1}{2} + O(\epsilon) \right], \end{aligned} \quad (9)$$

where ζ is Riemann's zeta function, with values $\zeta(2) = \pi^2/6$ and $\zeta(3) \approx 1.202\,056\,903$, and Cl_2 is Clausen's integral, with value $\text{Cl}_2(\pi/3) \approx 1.014\,941\,606$.

In the remainder of this section, we describe the evaluation of the finite diagrams \mathcal{I}_1 through \mathcal{K}_2 . This is achieved with the help of the methods developed in Refs. [24,25,26,27]. These methods suggest a separation of the integration space in an orthogonal and a parallel space. The parallel space is defined to be the linear span of the exterior momenta involved in the process under consideration. For a three-point function, this is a two-dimensional space. Each loop momentum is a sum of two vectors, one being its projection onto the two-dimensional plane spanned by two non-degenerate exterior momenta, the other one being orthogonal to this plane. This splitting does not break Lorentz invariance [28]. In the following, we define orthogonal- and parallel-space variables for our purposes. We assume two independent exterior momenta, p_1 and p_2 , and two loop momenta, l and k . Without loss of generality, we assume p_1 and p_2 to be timelike. Then, $e_1 = p_1/\sqrt{p_1^2}$ and $e_2 = (p_2 - p_2 \cdot e_1 e_1)/\sqrt{(p_2 \cdot e_1)^2 - p_2^2}$ are orthogonal unit vectors, with $e_1^2 = -e_2^2 = 1$ and $e_1 \cdot e_2 = 0$. We further define

$$\begin{aligned} l_0 &= l \cdot e_1, \\ k_0 &= k \cdot e_1, \\ l_1 &= l \cdot e_2, \\ k_1 &= k \cdot e_2, \\ l_\perp &= l - l_0 e_1 - l_1 e_2, \\ k_\perp &= k - k_0 e_1 - k_1 e_2. \end{aligned} \quad (10)$$

We then have

$$\begin{aligned}
e_i \cdot l_\perp &= 0, \\
e_i \cdot k_\perp &= 0, \\
l^2 &= l_0^2 - l_1^2 - l_\perp^2, \\
k^2 &= k_0^2 - k_1^2 - k_\perp^2, \\
l \cdot p_1 &= l_0 p_1 \cdot e_1, \\
k \cdot p_1 &= k_0 p_1 \cdot e_1, \\
l \cdot p_2 &= l_0 p_2 \cdot e_1 - l_1 p_2 \cdot e_2, \\
k \cdot p_2 &= k_0 p_2 \cdot e_1 - k_1 p_2 \cdot e_2, \\
l \cdot k &= l_0 k_0 - l_1 k_1 - l_\perp \cdot k_\perp, \\
(l+k)^2 &= (l_0+k_0)^2 - (l_1+k_1)^2 - l_\perp^2 - k_\perp^2 - 2l_\perp \cdot k_\perp.
\end{aligned} \tag{11}$$

Futhermore, we call the angle between the two-loop momenta in orthogonal space

$$z = \frac{l_\perp \cdot k_\perp}{\sqrt{l_\perp^2 k_\perp^2}}. \tag{12}$$

In its most straightforward application, this approach delivers a two-fold integral representation for the two-loop two-point function [25]. Typically, the remaining integrations are with respect to the parallel-space component of each of the two loop momenta.

For two-loop three-point functions [26], and for four-point functions as well [29], this approach opens a route to three-fold integral representations, regardless of the internal topology of the function. In Ref. [27], this was improved to give a two-fold integral representation for the planar three-point case. Remarkably, the so-obtained integral representations are solely defined on finite domains of integration [27]. These results are sufficient to treat topologies \mathcal{J}_i and, with slight modifications, topologies \mathcal{I}_i as well. A similar result for the three-point non-planar case was obtained recently [30], and was used here for the first time to handle topologies \mathcal{K}_i .

We now wish to describe some features of the method. Following separation into parallel-space and orthogonal-space variables, the angular integration in the orthogonal space is complicated due to the presence of propagators involving both loop momenta, which results in a non-trivial integration over the variable z . In fact, the z integration delivers a result of the form $f(P_i |_{l_\perp=k_\perp=0})$, where f is a function having a single branch-cut and P_i is such a propagator involving both loop momenta. In f , this propagator is evaluated at nullified orthogonal loop momenta. Typically, in four-dimensional field theory, f turns out to be a logarithm in the two-loop two-point case, and a square root in the two-loop three-point case.

By the very definition of a scalar field propagator, P_i is a quadratic form in parallel-space variables. Parallel-space integrations over the real line are most conveniently performed with the help of the residue theorem. To this end, we wish to close the contour in either the upper or the lower halfplane. This is obscured by the cut of $f(P_i |_{l_\perp=k_\perp=0})$,

which is present in both halfplanes. The problem is readily solved by using translations $l_0 \rightarrow l_0 + l_1$ and $k_0 \rightarrow k_0 + k_1$. Using the $(+, -, -, -)$ signature of space-time, we see that these translations render the propagators linear in the variables l_1 and k_1 . Accordingly, the cut defined by the equation

$$f(l_1, k_1) = f(P_i |_{l_\perp=k_\perp=0}) = -c, \quad (13)$$

with $c > 0$, is now in either the lower or upper complex l_1 (resp. k_1) plane. This allows us to close the contour in the opposite halfplane. The precise location of the cut becomes a function of the other integration variables. This results in constraint equations for the contributing residues, and thus in constraints on the domains of integration for the remaining variables. These domains turn out to be restricted to triangles in the (l_0, k_0) plane in the case of two-loop three-point functions [27,30].

At this stage, one is left with a four-fold integral representation. There are two integrations for the remaining parallel-space variables l_0 and k_0 , and the moduli $s = l_\perp^2$ and $t = k_\perp^2$ still have to be integrated over the positive real axis. These last two integrations can be carried out next. These s and t integrals have the form [27,30]

$$\int_0^\infty dt \frac{1}{t + t_0 \pm i\eta} \int_0^\infty ds \frac{1}{s + s_0(t) \pm i\eta} \frac{1}{\sqrt{(at + b + i\eta + cs)^2 - 4st}}, \quad (14)$$

with the cut of the square root chosen to be along the positive real axis. The coefficients are functions of the parallel space variables l_0 and k_0 . With due care to the analytic structure of the integrand, one achieves the first integration by using either Landen [26] or Euler transformations [27,30]. The results allow one to interpret the t integration as an integral representation of dilogarithms and associated functions, and thus one obtains a two-fold integral representation as the final result. We once more stress that the final two integrations only cover finite triangular domains. They are suitable for numerical integrations using Gaussian quadrature.

This programme was first successfully applied to two-loop three-point functions in Ref. [27], and then extended to the crossed topology in Ref. [30]. For the crossed topology, the unavoidable presence of two propagators involving both loop momenta results in a more complicated cut structure. There are many more cases to be considered, but the calculation still follows the scheme outlined above.

4 Results

We now present our results for diagrams \mathcal{F}_1 through \mathcal{K}_2 in the form of Eq. (6). The number of propagators is $N = 4$ for \mathcal{F}_i , $N = 5$ for \mathcal{G}_i and \mathcal{I}_i , and $N = 6$ for \mathcal{H}_i , \mathcal{J}_i , and \mathcal{K}_i . Coefficients A , B , and C are listed in Tables 1 and 2. The formulas for coefficients C of \mathcal{F}_2 , \mathcal{G}_5 , and \mathcal{H}_5 are somewhat lengthy, and we have introduced the following constants:

$$F_2 = -\frac{4}{5}\zeta(3) + \zeta(2) \left(-\frac{2}{5} \ln \frac{3 - \sqrt{5}}{2} - 4 \ln \frac{\sqrt{5} - 1}{2} + \frac{6}{\sqrt{5}} + \frac{7}{2} \right) + \frac{1}{12} \ln^3 \frac{3 - \sqrt{5}}{2}$$

$$\begin{aligned}
& -\frac{2}{3} \ln^3 \frac{\sqrt{5}-1}{2} + (\sqrt{5}-1) \left(\frac{1}{2} \ln^2 \frac{3-\sqrt{5}}{2} - 2 \ln^2 \frac{\sqrt{5}-1}{2} \right) - \frac{19}{2} \\
& \approx 3.508\,941\,259, \\
f_2 &= 4 \ln^2 \frac{\sqrt{5}-1}{2} - 2\sqrt{5} \ln \frac{\sqrt{5}-1}{2} - 5 \\
& \approx -1.921\,696\,013, \\
G_5 &= \int_0^{1/4} dx \frac{\sqrt{1-4x}}{x(1-x)} [\text{Li}_2(-x) + \ln x \ln(1+x)] \\
& \approx -0.647\,466\,172, \\
g_5 &= -\int_0^{1/4} dx \frac{\sqrt{1-4x}}{x(1-x)} \ln(1+x) \\
&= \sqrt{3} \left[\text{Cl}_2 \left(\frac{2}{3}\pi + \arctan \sqrt{15} \right) + \text{Cl}_2 \left(\frac{2}{3}\pi - \arctan \sqrt{15} \right) \right] - \frac{4}{\sqrt{3}} \text{Cl}_2 \left(\frac{\pi}{3} \right) \\
&\quad - 2 \ln^2 \frac{\sqrt{5}-1}{2} + \frac{\pi}{\sqrt{3}} \ln 2 \\
& \approx -0.177\,283\,264, \\
H_5 &= \int_0^{1/4} dx \frac{\sqrt{1-4x}}{(1-x)^2} [\text{Li}_2(-x) + \ln x \ln(1+x)] \\
& \approx -0.065\,325\,931, \\
h_5 &= -\int_0^{1/4} dx \frac{\sqrt{1-4x}}{(1-x)^2} \ln(1+x) \\
&= -\frac{2}{\sqrt{3}} \left[\text{Cl}_2 \left(\frac{2}{3}\pi + \arctan \sqrt{15} \right) + \text{Cl}_2 \left(\frac{2}{3}\pi - \arctan \sqrt{15} \right) \right] + \frac{8}{3\sqrt{3}} \text{Cl}_2 \left(\frac{\pi}{3} \right) \\
&\quad - \frac{\sqrt{5}}{2} \ln \frac{3-\sqrt{5}}{2} - \frac{\pi}{\sqrt{3}} \left(\frac{2}{3} \ln 2 + \frac{1}{2} \right) \\
& \approx -0.021\,441\,581. \tag{15}
\end{aligned}$$

The analytic results for G_5 and H_5 are rather messy, and we refrain from writing them down here.

In Sec. 3, we discussed the elimination of the IR-divergent pieces in Eq. (3). Substituting in the remainder of Eq. (3) the expressions for δM_H^2 , Z_w , Z_H , λ_0 , and v_0 in terms of M_H and λ [19] as well as the results for the various one- and two-loop diagrams, we may set $\epsilon = 0$ and so obtain the physical result

$$\begin{aligned}
\mathcal{T}(H \rightarrow VV) &= -2\lambda v \left\{ 1 + \hat{\lambda} \left[5\zeta(2) - 3\pi\sqrt{3} + \frac{19}{2} + i\pi(2\ln 2 - 5) \right] \right. \\
&+ \hat{\lambda}^2 \left[-2\zeta(3) + \zeta(2) \left(-45\pi\sqrt{3} + 144\ln 2 + \frac{1173}{2} \right) + 4(33\sqrt{3} + 4\pi) \text{Cl}_2 \left(\frac{\pi}{3} \right) \right. \\
&\quad - 181\pi\sqrt{3} - \frac{749}{8} + 189L_5 - 2F_2 - 12G_5 - 18H_5 \\
&\quad \left. \left. + 12I_1 + 12I_2 + 8I_3 + 72I_4 + 40I_5 + 24I_6 + 8I_7 \right] \right\}
\end{aligned}$$

$$\begin{aligned}
& + 108J_1 + 12J_2 + 12J_3 + 4J_4 + 72J_5 + 24J_6 + 24J_7 + 8J_8 + 36K_1 + 4K_2 \\
& + i \left(\zeta(2) \left(-108\sqrt{3}\ln 2 + 174\sqrt{3} - 53\pi \right) + \pi \left(57\ln 2 - \frac{41}{2} - 2f_2 - 12g_5 - 18h_5 \right) \right. \\
& \left. + 40i_5 + 8i_7 + 12j_2 + 12j_3 + 4j_4 + 24j_7 + 8j_8 + 4k_2 \right) \Big] \Big\}, \tag{16}
\end{aligned}$$

where $\hat{\lambda} = \lambda/(16\pi^2) = G_F M_H^2/(16\pi^2\sqrt{2})$. Here, $L_5 \approx 0.923\,631\,827$ stems from the all-massive lemon diagram, $\mathcal{L}_5 = L_5/[(4\pi)^4 M_H^2] + O(\epsilon)$, and is given in terms of a two-dimensional integral in Eq. (A86) of Ref. [19], where it is called K_5 . All other constants are listed in Tables 1 and 2 together with Eq. (15). Inserting in Eq. (16) the numerical values of these constants, we find

$$\begin{aligned}
\mathcal{T}(H \rightarrow VV) \approx & -2\lambda v \left\{ 1 + \hat{\lambda}(1.400\,476 - 11.352\,791\,i) \right. \\
& \left. - \hat{\lambda}^2[34.408\,2(43) + 21.003\,1(62)\,i] \right\}. \tag{17}
\end{aligned}$$

This agrees reasonably well with Eq. (13) of Ref. [18], where the two-loop coefficient is found to be $-[34.351(26) + 20.999(20)\,i]$. Taking the absolute squared of Eq. (17), we obtain the correction factor, K_V , in the relation $\Gamma(H \rightarrow VV) = K_V \Gamma_B(H \rightarrow VV)$ between the radiatively corrected and Born values of the $H \rightarrow VV$ decay width as

$$\begin{aligned}
K_V \approx & 1 + 2.800\,952\,\hat{\lambda} + 62.030\,8(86)\,\hat{\lambda}^2 \\
\approx & 1 + 14.629\% \left(\frac{M_H}{1\,\text{TeV}} \right)^2 + 16.921(2)\% \left(\frac{M_H}{1\,\text{TeV}} \right)^4. \tag{18}
\end{aligned}$$

For comparison, we also list the analogous correction factor, $K_f = \Gamma(H \rightarrow f\bar{f})/\Gamma_B(H \rightarrow f\bar{f})$, for the Higgs-boson decay to a pair of fermions [13,14]:

$$K_f \approx 1 + 11.058\% \left(\frac{M_H}{1\,\text{TeV}} \right)^2 - 8.908\% \left(\frac{M_H}{1\,\text{TeV}} \right)^4. \tag{19}$$

In the derivation of Eq. (19), Yukawa couplings have been set to zero. Therefore Eq. (19) should be a useful approximation to the full electroweak two-loop result as long as $M_f \ll M_H$.

5 Discussion and conclusions

We are now in a position to explore the phenomenological consequences of our result. In Fig. 2, we display the $H \rightarrow VV$ correction factor K_V of Eq. (18) to $O(G_F M_H^2)$ and $O(G_F^2 M_H^4)$ as a function of M_H . For comparison, also the corresponding approximations for the $H \rightarrow f\bar{f}$ correction factor K_f of Eq. (19) are shown. In both cases, the $O(G_F M_H^2)$ terms enhance the Born results. This effect is slightly more pronounced for K_V . In the case of K_V , the $O(G_F^2 M_H^4)$ term acts in the same direction as the $O(G_F M_H^2)$ term. For M_H increasing, it rapidly gains importance relative to the $O(G_F M_H^2)$ term; at $M_H \approx 930\,\text{GeV}$,

both terms have the same numerical value, 12.6%. In the case of K_f , the $O(G_F^2 M_H^4)$ term reduces and, for $M_H \gtrsim 1.114$ TeV, overcompensates the effect of the $O(G_F M_H^2)$ term. Obviously, the perturbation expansions of K_V and K_f in $G_F M_H^2$ cease to usefully converge for M_H values in excess of about 1 TeV. Consequently, this value may be considered as an upper bound on the Higgs-boson pole mass M_H , if the SM is to be weakly interacting [9]. We emphasize that this observation is independent of speculations concerning the energy scale up to which the SM is supposed to be valid.

The Goldstone-boson equivalence theorem [17] allowed us to extract power corrections in $G_F M_H^2$. In the high- M_H limit, these are clearly dominant over corrections in $G_F M_W^2$ and $G_F M_t^2$ arising from the gauge and Yukawa sectors of the SM, respectively. For the $H \rightarrow W^+W^-$ and $H \rightarrow ZZ$ decays, this was verified for the $O(G_F M_H^2)$ terms in Refs. [31,32], where the respective partial widths were completely calculated to one loop in the SM. There is no obvious reason why the situation should be different at the electroweak two-loop order. QCD corrections enter the stage only at the two-loop level, in connection with quark loops. The dominant two- and three-loop QCD corrections to the W^+W^-H and ZZH couplings, of $O(\alpha_s G_F M_t^2)$ [33] and $O(\alpha_s^2 G_F M_t^2)$ [34], respectively, are well under control and suppressed against the $G_F M_H^2$ power corrections for M_H large. The dominance of the $G_F M_H^2$ power corrections in the case of the $f\bar{f}H$ Yukawa couplings was discussed in great detail in Refs. [13,35]. In this context, we should mention that the $O(G_F M_H^2)$ two-loop corrections to the partial width of the loop-induced $H \rightarrow \gamma\gamma$ decay have been computed [36] with the aid of the Goldstone-boson equivalence theorem.

Since a Higgs boson with mass $M_H \gg 2M_Z$ decays almost exclusively to pairs of intermediate bosons and top quarks, and we have gained control over the dominant two-loop corrections to the respective partial widths, we are now able to predict the lifetime of a high-mass Higgs boson with two-loop precision. For the reader's convenience, we list here the Born formulas of the relevant partial decay widths:

$$\begin{aligned}\Gamma_B(H \rightarrow W^+W^-) &= \frac{G_F M_H^3}{8\pi\sqrt{2}}(1 - r_W)^{1/2} \left(1 - r_W + \frac{3}{4}r_W^2\right), \\ \Gamma_B(H \rightarrow ZZ) &= \frac{G_F M_H^3}{16\pi\sqrt{2}}(1 - r_Z)^{1/2} \left(1 - r_Z + \frac{3}{4}r_Z^2\right), \\ \Gamma_B(H \rightarrow t\bar{t}) &= \frac{N_c G_F M_H^3}{16\pi\sqrt{2}}r_t(1 - r_t)^{3/2},\end{aligned}\tag{20}$$

where $N_c = 3$ and $r_a = 4M_a^2/M_H^2$ ($a = W, Z, t$). We compute the total Higgs-boson decay width as

$$\Gamma_H = K_V \left[\Gamma_B(H \rightarrow W^+W^-) + \Gamma_B(H \rightarrow ZZ) \right] + K_f \Gamma_B(H \rightarrow t\bar{t}).\tag{21}$$

We display the result as a function of M_H in Fig. 3, assuming $M_t = 175$ GeV. Comparing the Born, one-loop, and two-loop approximations, the significance of radiative corrections to the heavy-Higgs lifetime, $\tau_H = 1/\Gamma_H$, becomes evident.

Equations (18), (19), and (20) refer to the on-mass-shell renormalization scheme and are thus independent of the unphysical renormalization scale μ , which enters via dimensional regularization. By contrast, in other renormalization schemes such as the $\overline{\text{MS}}$

scheme, there remains a weak μ dependence in the loop-corrected expressions for the various Higgs-boson decay widths. It is generally believed that the scheme and scale dependences of a calculation up to a given order indicate the size of the unknown higher-order contributions, *i.e.*, they provide us with an estimate of the theoretical uncertainty. Applying this empirical rule to the fermionic and bosonic Higgs-boson decays, one may conclude that the respective perturbative results are likely to become unreliable already for $M_H \gtrsim 700$ GeV [37,38]. In fact, for $M_H \gtrsim 700$ GeV, the μ dependences of the $\overline{\text{MS}}$ results are no longer reduced if the two-loop corrections are included [38].

Finally, we should mention that Monte-Carlo studies on finite lattices provide us with a hint on the all-order relation between the mass and the bosonic decay width of the Higgs boson [39,40]. In Ref. [39], elastic $\pi\pi$ scattering was analyzed nonperturbatively in the framework of the four-dimensional $O(4)$ -symmetric nonlinear σ model in the broken phase, and the σ resonance was observed. The mass m_σ and width Γ_σ of this resonance could be extracted from the measured scattering phases. At the same time, the pion mass m_π and wave-function-renormalization constant Z as well as the field expectation value Σ in infinite volume were determined. In this way, it is possible to compare the nonperturbative value of Γ_σ with the respective perturbative value obtained by inserting m_π , m_σ , Z , and Σ into the tree-level formula for Γ_σ , given by Eqs. (9.4) and (9.5) of Ref. [39]. For the central simulation point, the nonperturbative result is found to exceed the tree-level one by approximately 16.7% [41]. It is interesting to confront this all-order correction with the one- and two-loop corrections of Eq. (18). If we identify m_σ , Z , and Σ of Ref. [39] with our parameters M_H , Z_w , and v_0 , respectively, we have $2\lambda = (M_H/v)^2 = Z(m_\sigma/\Sigma)^2$, where the lattice constant cancels on the right-hand side. We so find that the central simulation point of Ref. [39] corresponds to $M_H \approx 727$ GeV, for which the corrections through $O(G_F M_H^2)$ and $O(G_F^2 M_H^4)$ in Eq. (18) amount to approximately 7.7% and 12.5%, respectively. The tree-level, one-loop, two-loop, and nonperturbative values of K_V at this value of M_H are indicated by the crosses in Fig. 2. In other words, the one- and two-loop terms of K_V are 7.7% and 4.7%, respectively, while the higher-order terms apparently add up to a total of 4.3%. This is a very reasonable result, which gives support to the notion that the perturbative expansion in $G_F M_H^2$ of the bosonic Higgs-decay width is still usefully convergent for this value of M_H , in accordance with the conclusions drawn above on the basis of Fig. 2. However, this observation should be taken with a grain of salt. The analysis of Ref. [39] was performed with m_π finite, while we set $M_w = 0$ for the Goldstone-boson pole mass. Nevertheless, we believe that such finite-mass effects will not drastically change our conclusions as long as we compare the relative corrections to the decay widths rather than the absolute values of the latter. This assumption is substantiated by the detailed inspection of the full one-loop results for the $H \rightarrow W^+W^-$ and $H \rightarrow ZZ$ partial decay widths [31,32].

ACKNOWLEDGEMENTS

We thank A. Ghinculov for providing us with some partial results of Ref. [18], and M. Göckeler, M. Lüscher, P. Weisz, and J. Westphalen for valuable advice regarding the comparison of our result with Ref. [39]. The collaboration on this project was initiated

during the Workshop on *Higher Order Perturbative Corrections in the Standard Model at the Aspen Center for Physics*.

A Appendix: One-loop three-point diagrams

Here, we present the relevant one-loop three-point diagrams to $O(\epsilon)$. We write the generic one-loop three-point integral as

$$\begin{aligned} & \mathcal{C}(p^2, k^2, (p+k)^2, m_1^2, m_2^2, m_3^2) \\ &= \mu^{2\epsilon} \int \frac{d^D q}{(2\pi)^D} \frac{1}{(q^2 - m_1^2 + i\epsilon)[(q+p)^2 - m_2^2 + i\epsilon][(q+p+k)^2 - m_3^2 + i\epsilon]}. \end{aligned} \quad (22)$$

The one-loop three-point diagrams in Fig. 1 are then defined as

$$\begin{aligned} \mathcal{C}_1 &= \mathcal{C}(0, 0, M_H^2, 0, M_H^2, 0), \\ \mathcal{C}_2 &= \mathcal{C}(0, 0, M_H^2, M_H^2, 0, M_H^2), \\ \mathcal{D}_1 &= \frac{\partial}{\partial m_1^2} \mathcal{C}(0, 0, M_H^2, 0, M_H^2, 0), \\ \mathcal{D}_{2a} &= \frac{\partial}{\partial m_2^2} \mathcal{C}(0, 0, M_H^2, 0, M_H^2, 0), \\ \mathcal{D}_{2b} &= \frac{\partial}{\partial m_2^2} \mathcal{C}(0, 0, M_H^2, M_H^2, 0, M_H^2), \\ \mathcal{D}_3 &= \frac{\partial}{\partial m_1^2} \mathcal{C}(0, 0, M_H^2, M_H^2, 0, M_H^2). \end{aligned} \quad (23)$$

We find

$$\begin{aligned} \mathcal{C}_1 &= \frac{i}{(4\pi)^2 M_H^2} \left(\frac{4\pi\mu^2}{M_H^2 e^\gamma} \right)^\epsilon \left\{ -\frac{\zeta(2)}{2} - i\pi \ln 2 \right. \\ & \quad \left. + \epsilon \left[-\frac{19}{8}\zeta(3) + \frac{9}{2}\zeta(2) \ln 2 + i\pi \left(-\zeta(2) + \frac{\ln^2 2}{2} \right) \right] + O(\epsilon^2) \right\}, \\ \mathcal{C}_2 &= \frac{i}{(4\pi)^2 M_H^2} \left(\frac{4\pi\mu^2}{M_H^2 e^\gamma} \right)^\epsilon \left\{ -\frac{2}{3}\zeta(2) + \epsilon \left[\frac{2}{9}\zeta(3) - \frac{4\pi}{9} \text{Cl}_2 \left(\frac{\pi}{3} \right) \right] + O(\epsilon^2) \right\}, \\ \mathcal{D}_{2a} &= \frac{i}{(4\pi)^2 M_H^4} \left(\frac{4\pi\mu^2}{M_H^2 e^\gamma} \right)^\epsilon \left\{ i\frac{\pi}{2} + \epsilon \left[-\frac{5}{4}\zeta(2) + i\frac{3\pi}{2} \ln 2 \right] + O(\epsilon^2) \right\}, \\ \mathcal{D}_3 &= \frac{i}{(4\pi)^2 M_H^4} \left(\frac{4\pi\mu^2}{M_H^2 e^\gamma} \right)^\epsilon \left\{ \frac{\pi}{3\sqrt{3}} + \epsilon \left[\frac{2}{3}\zeta(2) + \frac{4}{3\sqrt{3}} \text{Cl}_2 \left(\frac{\pi}{3} \right) - \frac{\pi}{3\sqrt{3}} \ln 3 \right] + O(\epsilon^2) \right\}. \end{aligned} \quad (24)$$

As already stated in Sec. 3, \mathcal{D}_1 and \mathcal{D}_{2b} are IR divergent. We need not calculate them, since their prefactors in Eq. (3) vanish according to Eq. (9).

References

- [1] J.-F. Grivaz, in *Proceedings of the International Europhysics Conference on High Energy Physics*, Brussels, Belgium, July 27–August 2, 1995, to appear.
- [2] E. Gross, B.A. Kniehl, and G. Wolf, *Z. Phys. C* **63**, 417 (1994); **66**, 321(E) (1995); M. Carena, P.M. Zerwas, *et al.*, in *Physics at LEP2*, edited by G. Altarelli, T. Sjostrand, and F. Zwirner, CERN Yellow Report No. 96–01, Vol. 1 (February 1996) p. 351.
- [3] A.D. Linde, *Pis'ma Zh. Eksp. Teor. Fiz.* **23**, 73 (1976) [*JETP Lett.* **23**, 64 (1976)]; S. Weinberg, *Phys. Rev. Lett.* **36**, 294 (1976); M.J. Duncan, R. Philippe, and M. Sher, *Phys. Lett.* **153B**, 165 (1985); M. Sher, *Phys. Rep.* **179**, 273 (1989); *Phys. Lett. B* **317**, 159 (1993); **331**, 448(A) (1994); M. Lindner, M. Sher, and H.W. Zaglauer, *Phys. Lett. B* **228**, 139 (1989); C. Ford, D.R.T. Jones, P.W. Stephenson, and M.B. Einhorn, *Nucl. Phys.* **B395**, 17 (1993); G. Altarelli and G. Isidori, *Phys. Lett. B* **337**, 141 (1994); J.A. Casas, J.R. Espinosa, and M. Quiros, *Phys. Lett. B* **342**, 171 (1995).
- [4] D.A. Dicus and V.S. Mathur, *Phys. Rev. D* **7**, 3111 (1973); B.W. Lee, C. Quigg, and H.B. Thacker, *Phys. Rev. Lett.* **38**, 883 (1977); *Phys. Rev. D* **16**, 1519 (1977).
- [5] L. Durand, J.M. Johnson, and J.L. Lopez, *Phys. Rev. Lett.* **64**, 1215 (1990); *Phys. Rev. D* **45**, 3112 (1992).
- [6] L. Durand, P.N. Maher, and K. Riesselmann, *Phys. Rev. D* **48**, 1084 (1993).
- [7] N. Cabibbo, L. Maiani, G. Parisi, and R. Petronzio, *Nucl. Phys.* **B158**, 295 (1979); M. Lindner, *Z. Phys. C* **31**, 295 (1986).
- [8] R. Dashen and H. Neuberger, *Phys. Rev. Lett.* **50**, 1897 (1983); W. Langguth and I. Montvay, *Z. Phys. C* **36**, 725 (1987); A. Hasenfratz, T. Neuhaus, K. Jansen, H. Yoneyama, and C.B. Lang, *Phys. Lett. B* **199**, 531 (1987); A. Hasenfratz and T. Neuhaus, *Nucl. Phys.* **B297**, 205 (1988); P. Hasenfratz and J. Nager, *Z. Phys. C* **37**, 477 (1988); M. Lüscher and P. Weisz, *Phys. Lett. B* **212**, 472 (1988); U.M. Heller, H. Neuberger, and P. Vranas, *Nucl. Phys.* **B399**, 271 (1993); U.M. Heller, M. Klomfass, H. Neuberger, and P. Vranas, *Nucl. Phys.* **B405**, 555 (1993).
- [9] M. Veltman, *Phys. Lett.* **70B**, 253 (1977).
- [10] M. Veltman, *Acta Phys. Pol. B* **8**, 475 (1977).
- [11] W.J. Marciano and S.S.D. Willenbrock, *Phys. Rev. D* **37**, 2509 (1988).
- [12] B.A. Kniehl, *Phys. Rep.* **240**, 211 (1994).
- [13] L. Durand, B.A. Kniehl, and K. Riesselmann, *Phys. Rev. Lett.* **72**, 2534 (1994); **74**, 1699(E) (1995); *Phys. Rev. D* **51**, 5007 (1995).

- [14] A. Ghinculov, Phys. Lett. B **337**, 137 (1994); **346**, 426(E) (1995).
- [15] K. Riesselmann, Phys. Rev. D **53**, 6226 (1996).
- [16] K. Riesselmann and S. Willenbrock, Report Nos. ILL-(TH)-96-4 and TUM-HEP-236/96 (June 1996).
- [17] J.M. Cornwall, D.N. Levin, and G. Tiktopoulos, Phys. Rev. D **10**, 1145 (1974); **11**, 972(E) (1975); C.E. Vayonakis, Lett. Nuovo Cim. **17**, 383 (1976); M.S. Chanowitz and M.K. Gaillard, Nucl. Phys. **B261**, 379 (1985); G.J. Gounaris, R. Kögerler, and H. Neufeld, Phys. Rev. D **34**, 3257 (1986); Y.-P. Yao and C.-P. Yuan, Phys. Rev. D **38**, 2237 (1988); J. Bagger and C. Schmidt, Phys. Rev. D **41**, 264 (1990); H. Veltman, Phys. Rev. D **41**, 2294 (1990); H.-J. He, Y.-P. Kuang, and X. Li, Phys. Rev. Lett. **69**, 2619 (1992); Phys. Rev. D **49**, 4842 (1994); H.-J. He, Y.-P. Kuang, and C.-P. Yuan, Phys. Rev. D **51**, 6463 (1995).
- [18] A. Ghinculov, Nucl. Phys. **B455**, 21 (1995).
- [19] P.N. Maher, L. Durand, and K. Riesselmann, Phys. Rev. D **48**, 1061 (1993); **52**, 553(E) (1995).
- [20] A. Ghinculov and J.J. van der Bij, Nucl. Phys. **B436**, 30 (1995).
- [21] J.M. Johnson, Ph.D. thesis, University of Wisconsin-Madison (1990).
- [22] N.I. Ussyukina and A.I. Davydychev, Phys. Lett. B **332**, 159 (1994). A misprint in Eq. (24) is corrected in Phys. Lett. B **348**, 503 (1995).
- [23] B.A. Kniehl, Phys. Lett. B **237**, 127 (1990); Phys. Lett. B **343**, 299 (1995).
- [24] D. Kreimer, talk given at *Workshop on High Energy Physics and Quantum Field Theory*, Sochi, Russia (1992); Yad. Fiz. **56**, 160 (1993) [Phys. Atom. Nucl. **56**, 1546 (1993)].
- [25] D. Kreimer, Phys. Lett. B **273**, 277 (1991).
- [26] D. Kreimer, Phys. Lett. B **292**, 341 (1992).
- [27] A. Czarnecki, U. Kilian, and D. Kreimer, Nucl. Phys. **B433**, 259 (1995).
- [28] D. Kreimer, Mod. Phys. Lett. A **9**, 1105 (1994).
- [29] D. Kreimer, Phys. Lett. B **347**, 107 (1995).
- [30] A. Frink, Diploma thesis, University of Mainz (1996).
- [31] B.A. Kniehl, Nucl. Phys. **B357**, 439 (1991).
- [32] B.A. Kniehl, Nucl. Phys. **B352**, 1 (1991).

- [33] B.A. Kniehl and M. Spira, Nucl. Phys. **B443**, 37 (1995); Z. Phys. C **69**, 77 (1995).
- [34] B.A. Kniehl and M. Steinhauser, Nucl. Phys. **B454**, 485 (1995); Phys. Lett. B **365**, 297 (1996).
- [35] L. Durand and K. Riesselmann, TU Munich Report Nos. TUM-HEP-227/95 and hep-ph/9512224 (December 1995).
- [36] J.G. Körner, K. Melnikov, and O.I. Yakovlev, Phys. Rev. D **53**, 3737 (1996).
- [37] A.I. Bochkarev and R.S. Willey, Phys. Rev. D **51**, R2049 (1995).
- [38] U. Nierste and K. Riesselmann, Phys. Rev. D **53**, 6638 (1996).
- [39] M. Göckeler, H.A. Kastrup, J. Westphalen, and F. Zimmermann, Nucl. Phys. **B425**, 413 (1994).
- [40] K. Rummukainen and S. Gottlieb, Nucl. Phys. **B450**, 397 (1995).
- [41] M. Göckeler and J. Westphalen, private communication.

TABLES

Table 1: Coefficients A , B , and C to be inserted in template (6) to obtain the values of the divergent two-loop three-point diagrams of Fig. 1. $N = 4$ for \mathcal{F}_i , $N = 5$ for \mathcal{G}_i , and $N = 6$ for \mathcal{H}_i . Analytical and numerical results for F_2 , f_2 , G_5 , g_5 , H_5 , and h_5 are given in Eq. (15).

Graph	A	B	C
\mathcal{F}_1	$-\frac{1}{2}$	$-\frac{5}{2} - i\pi$	$\frac{11}{2}\zeta(2) - \frac{19}{2} - 5i\pi$
\mathcal{F}_2	$-\frac{1}{2}$	$-\frac{5}{2} - i\pi$	$F_2 + i\pi f_2$
\mathcal{F}_3	$-\frac{1}{2}$	$\frac{\pi}{\sqrt{3}} - \frac{5}{2}$	$\frac{8}{3}\zeta(3) - \frac{1}{3}\zeta(2) + \left(-\frac{2\pi}{3} + \frac{1}{\sqrt{3}}\right) \text{Cl}_2\left(\frac{\pi}{3}\right)$ $+ \frac{\pi}{\sqrt{3}}(-\ln 3 + 5) - \frac{19}{2}$
\mathcal{F}_4	$-\frac{1}{2}$	$-\frac{3}{2}$	$-\frac{5}{2}\zeta(2) - \frac{5}{2}$
\mathcal{F}_5	$-\frac{1}{2}$	$-\frac{3}{2}$	$-\frac{5}{4}\zeta(3) + 3\zeta(2)\left(\ln 2 - \frac{1}{2}\right) - \frac{5}{2}$
\mathcal{F}_6	$-\frac{1}{2}$	$-\frac{3}{2}$	$2\zeta(3) - \frac{1}{2}\zeta(2) - \frac{5}{2}$
\mathcal{G}_1	0	$\frac{2}{3}\zeta(2)$	$-\frac{11}{9}\zeta(3) + \frac{4}{3}\zeta(2)\left(-\frac{\pi}{3\sqrt{3}} + 1\right) + \frac{4\pi}{9} \text{Cl}_2\left(\frac{\pi}{3}\right)$
\mathcal{G}_2	0	$\frac{2}{3}\zeta(2)$	$\frac{1}{9}\zeta(3) + \frac{4}{3}\zeta(2) + \frac{4\pi}{9} \text{Cl}_2\left(\frac{\pi}{3}\right)$
\mathcal{G}_3	0	$\frac{1}{2}\zeta(2) + i\pi \ln 2$	$\frac{29}{8}\zeta(3) + \zeta(2)\left(-\frac{15}{2} \ln 2 + 1\right)$ $+ i\pi\left[\zeta(2) - \frac{1}{2} \ln^2 2 + \ln 2\right]$
\mathcal{G}_4	0	$\frac{2}{3}\zeta(2)$	$-\frac{26}{9}\zeta(3) - \frac{1}{6}\zeta(2) + \left(\frac{10\pi}{9} + \sqrt{3}\right) \text{Cl}_2\left(\frac{\pi}{3}\right)$
\mathcal{G}_5	0	$\frac{1}{2}\zeta(2) + i\pi \ln 2$	$\frac{19}{8}\zeta(3) + \zeta(2)\left(-\frac{\pi}{2\sqrt{3}} - \frac{9}{2} \ln 2 + 1\right) + G_5$ $+ i\pi\left[\zeta(2) - \frac{1}{2} \ln^2 2 + \left(-\frac{\pi}{\sqrt{3}} + 2\right) \ln 2 + g_5\right]$
\mathcal{G}_6	0	$\frac{1}{2}\zeta(2) + i\pi \ln 2$	$\frac{25}{8}\zeta(3) + \zeta(2)\left(-\frac{15}{2} \ln 2 + 1\right)$ $+ i\pi\left[\frac{3}{2}\zeta(2) - \frac{1}{2} \ln^2 2 + 2 \ln 2\right]$
\mathcal{H}_1	0	$-\frac{\pi}{3\sqrt{3}}$	$\zeta(2)\left(\frac{8\pi}{27\sqrt{3}} - \frac{3}{2}\right) + \frac{5}{3\sqrt{3}} \text{Cl}_2\left(\frac{\pi}{3}\right) + \frac{\pi}{3\sqrt{3}}(\ln 3 - 2)$
\mathcal{H}_2	0	$-\frac{\pi}{3\sqrt{3}}$	$-\frac{5}{6}\zeta(2) - \frac{7}{3\sqrt{3}} \text{Cl}_2\left(\frac{\pi}{3}\right) + \frac{\pi}{3\sqrt{3}}(\ln 3 - 2)$
$\mathcal{H}_3 - \mathcal{B}_1\mathcal{D}_1$	0	0	$\frac{3}{8}\zeta(2) - \frac{1}{2} + i\frac{\pi}{2} \ln 2$
$\mathcal{H}_4 - \mathcal{B}_1\mathcal{D}_{2b}$	0	0	$-\frac{1}{12}\zeta(2) - \frac{\sqrt{3}}{2} \text{Cl}_2\left(\frac{\pi}{3}\right) + \frac{\pi}{2\sqrt{3}} + \frac{1}{2}$
\mathcal{H}_5	0	$-i\frac{\pi}{2}$	$\zeta(2)\left(\frac{\pi}{3\sqrt{3}} + \frac{3}{4}\right) + H_5$ $+ i\pi\left[\left(\frac{2\pi}{3\sqrt{3}} - \frac{5}{2}\right) \ln 2 + \frac{\pi}{2\sqrt{3}} - 1 + h_5\right]$
\mathcal{H}_6	0	$-i\frac{\pi}{2}$	$\frac{9}{4}\zeta(2) - i\pi\left(\frac{5}{2} \ln 2 + 1\right)$

Table 2: Coefficients C to be inserted in template (6) to obtain the values of the finite two-loop three-point diagrams of Fig. 1 ($A = B = 0$). $N = 5$ for \mathcal{I}_i and $N = 6$ for \mathcal{J}_i and \mathcal{K}_i . The numerical uncertainties in the last digit(s) are given in parentheses.

Graph	C		
\mathcal{I}_1	I_1	$=$	$-1.894\,06(5)$
\mathcal{I}_2	I_2	$=$	$-2.004\,830(5)$
\mathcal{I}_3	I_3	$=$	$-3.652\,841(5)$
\mathcal{I}_4	I_4	$=$	$-1.280\,380(5)$
\mathcal{I}_5	$I_5 + i i_5$	$=$	$-1.352\,904(5) - 7.552\,73(3) i$
\mathcal{I}_6	I_6	$=$	$-1.921\,491(5)$
\mathcal{I}_7	$I_7 + i i_7$	$=$	$-2.137\,588(5) - 3.021\,09(3) i$
\mathcal{J}_1	J_1	$=$	$0.482\,636\,3(5)$
\mathcal{J}_2	$J_2 + i j_2$	$=$	$0.050\,486\,6(10) + 2.388\,03(6) i$
\mathcal{J}_3	$J_3 + i j_3$	$=$	$-0.829\,866(5) + 5.554\,50(3) i$
\mathcal{J}_4	$J_4 + i j_4$	$=$	$-3.890\,156(5) + 1.675\,52(3) i$
\mathcal{J}_5	J_5	$=$	$0.779\,304(10)$
\mathcal{J}_6	J_6	$=$	$2.067\,12(5)$
\mathcal{J}_7	$J_7 + i j_7$	$=$	$0.249\,480(10) + 2.103\,29(3) i$
\mathcal{J}_8	$J_8 + i j_8$	$=$	$-1.199\,53(5) + 5.567\,4(2) i$
\mathcal{K}_1	K_1	$=$	$0.607\,011(5)$
\mathcal{K}_2	$K_2 + i k_2$	$=$	$-1.211\,623(5) + 4.995\,5(3) i$

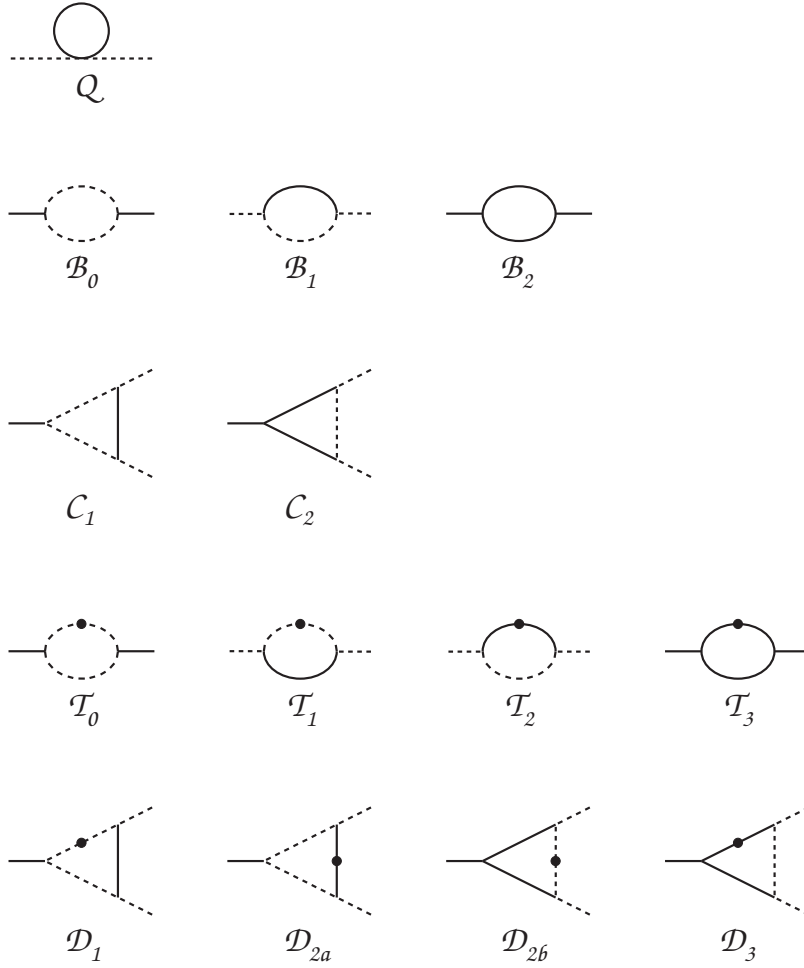


Figure 1: Feynman diagrams pertinent to the $H \rightarrow VV$ transition amplitude through $O(G_F^2 M_H^4)$. Dashed (solid) lines represent Goldstone (Higgs) bosons. Adjacent propagators with identical four-momenta are separated by a solid circle.

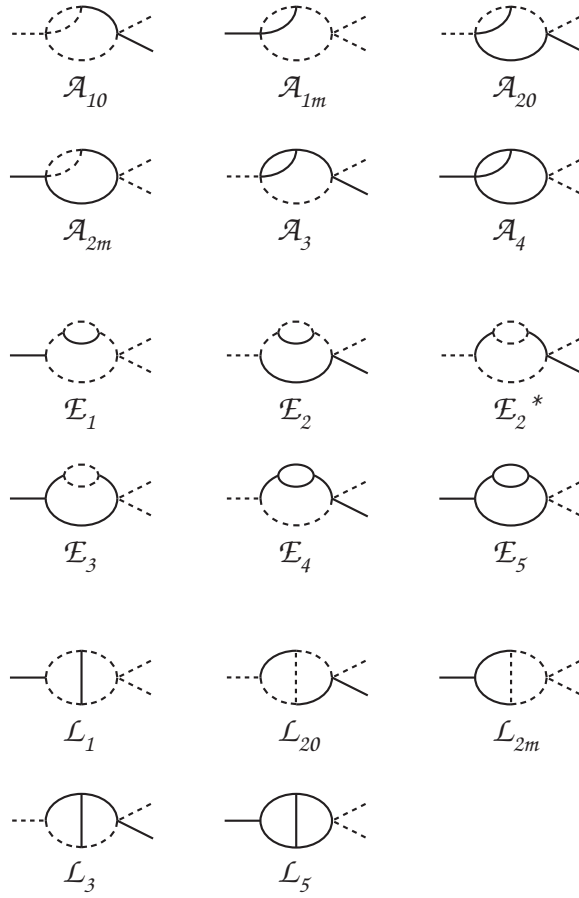


Figure 1: Continued.

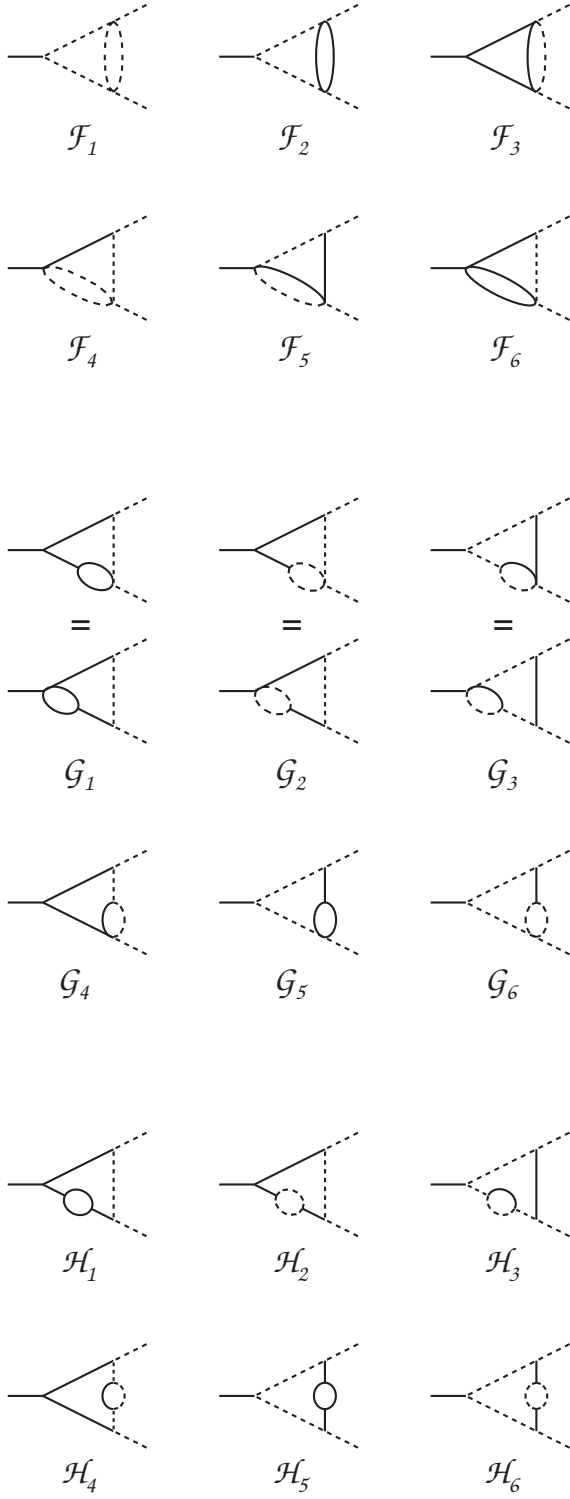


Figure 1: Continued.

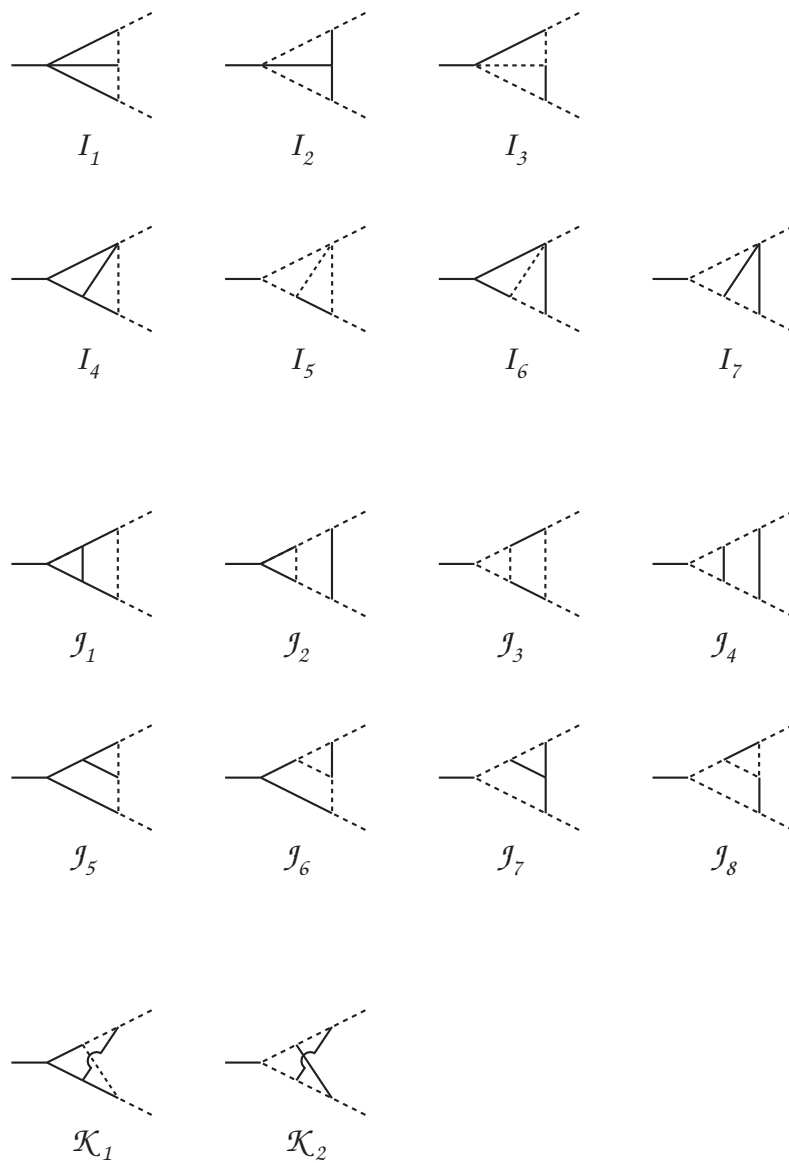


Figure 1: Continued.

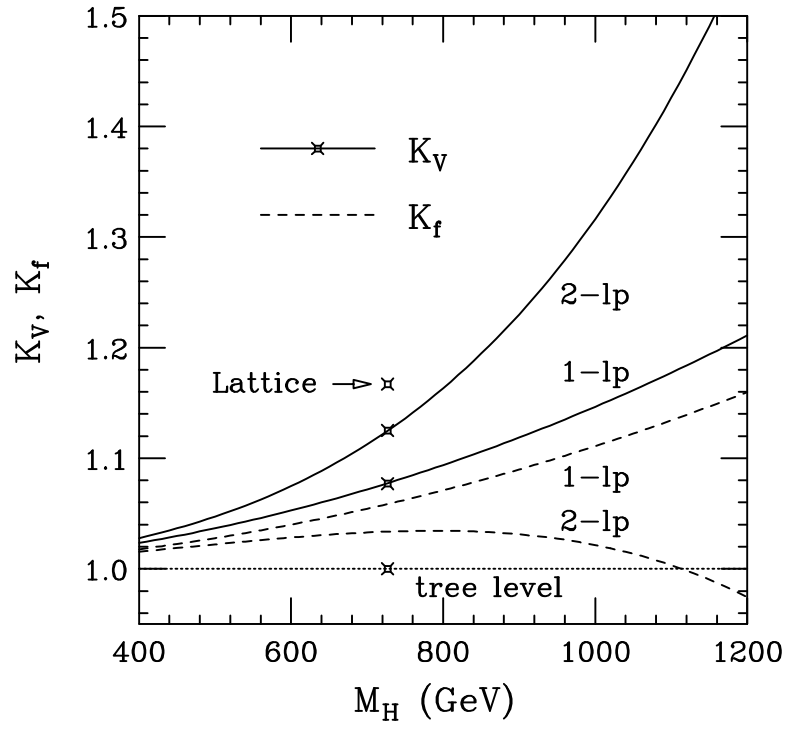


Figure 2: $H \rightarrow VV$ correction factor K_V of Eq. (18) to $O(G_F M_H^2)$ and $O(G_F^2 M_H^4)$ as a function of M_H (solid lines). For comparison, we also show the $H \rightarrow f\bar{f}$ correction factor K_f of Eq. (19) to $O(G_F M_H^2)$ and $O(G_F^2 M_H^4)$ (dashed lines). The crosses indicate the tree-level, one-loop, two-loop, and nonperturbative values of K_V at $M_H = 727$ GeV.

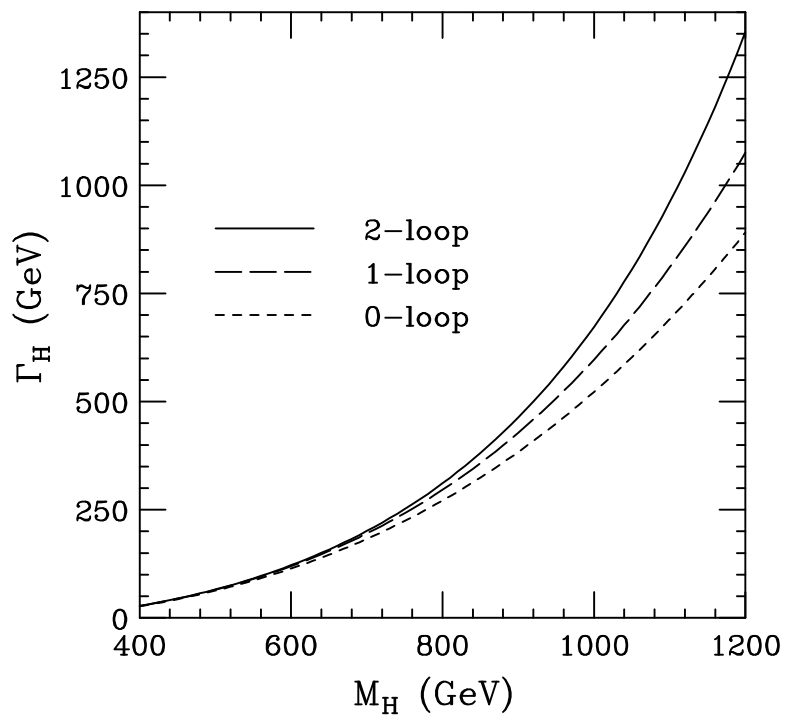


Figure 3: Total Higgs-boson decay width Γ_H in the Born approximation (short-dashed line), to $O(G_F M_H^2)$ (long-dashed line), and to $O(G_F^2 M_H^4)$ (solid line) as a function of M_H . We assume $M_t = 175$ GeV.